Computers & Fluids 47 (2011) 115–121

Contents lists available at ScienceDirect

Computers & Fluids

journal homepage: www.elsevier.com/locate/compfluid

Analysis of Lattice-Boltzmann methods for internal flows

Rainhill K. Freitas *, Andreas Henze, Matthias Meinke, Wolfgang Schröder

RWTH Aachen University, Institute of Aerodynamics, Wüllnerstr. 5a, 52062 Aachen, Germany

ARTICLE INFO

Article history:
Received 10 March 2008
Received in revised form 28 January 2011
Accepted 24 February 2011
Available online 3 March 2011

Keywords:
Lattice-Boltzmann
Wall turbulence
Direct numerical simulation
BGK
MRT
CLB

ABSTRACT

The applicability of several Lattice-Boltzmann methods to wall-bounded turbulent flows is investigated. The various methods consist of the standard Bhatnagar–Gross–Krook (BGK) method with 19 (BGK19) and 27 (BGK27) discrete velocities, the multiple-relaxation-time (MRT) model with 19 discrete velocities and the cascaded Lattice-Boltzmann method (CLB). Based on the findings of turbulent channel flow it can be concluded that stability considerations, predicting the superiority of the advanced moment based schemes like the CLB and MRT method not necessarily hold for wall-bounded turbulent flows. Moreover, in some flow problems the simple BGK method with 19 discrete velocities delivers reasonable and stable results, where the other methods yield unphysical solutions.

1. Introduction

Over the last 20 years the Lattice-Boltzmann method (LBM) has emerged as a new tool for computational fluid dynamics and has established its own constantly growing community. The method has some often cited special advantages, e.g., in the treatment of multiphase flows and complex geometries. The first applied and still most widely used LBM is the standard Bhatnagar–Gross–Krook (BGK) [1] method which is often favored because of its algorithmic simplicity. The drawback of the BGK is due to the stability behavior in medium to high Reynolds number flow regimes. To be more precise, the stability of the BGK method nonlinearly depends on the flow solution itself and on the collision frequency which is a function of the grid resolution and the viscosity. This means that the stability problems can be remedied, for instance, by a higher grid resolution or a finer discrete velocity representation.

However, there exist several other LBM methods in the literature to overcome these stability issues without using an extremely fine mesh resolution. Two of them being the MRT [2] and the CLB method [3]. There are other authors who investigated methods to stabilize LBM, like the entropic LB in Karlin et al. [7], Keating et al. [8] and the entropy limiter in Brownlee et al. [9]. The entropic LB was also used in Spasov et al. [10] to compute the turbulent channel flow. A high-order LB model using an entropy function is used in Chikatamarla et al. [11] to simulate a Kida vortex flow. These entropy methods are not an issue of the present work. The nonlinear nature of the LBM method, which is a consequence of the interdependence of the distribution functions and their moments, makes a rigorous stability analysis of the LBM a very challenging task. Therefore, benchmark simulations are still the most reliable way to investigate the stability bounds of LBM methods for turbulent flows. The MRT method has been applied, e.g., by Yu et al. [12] to investigate turbulent flows. Special attention has been spent to analyze decaying isotropic turbulence and incompressible subsonic jet flows. These studies proved the MRT to be a reliable tool to capture the effects of these unbounded cases. The CLB method proposed by Geier et al. [3] has been applied to calculate the turbulent wake of a rectangular obstacle showing good qualitative results. Further numerical analyses of the CLB method have been published in Geier et al. [4], Geier [5], and in Asinari [6].

This study focuses on wall-bounded turbulent flows, which encompass a vast number of flow problems. The turbulent flow in a channel containing obstacles using Lattice-Boltzmann equation was presented in Higuera et al. [13]. Amati et al. [14] as well as Toschi et al. [15] presented Lattice-Boltzmann results for turbulent channel flows at Reynolds numbers up to 3000. An early review on LBM is given in Benzi et al. [16]. In the context of the present work the performance of the standard BGK method with 19 and 27 discrete velocities, the MRT method with 19 discrete velocities, and the CLB method with 27 discrete velocities is discussed. Direct numerical simulations (DNS) with all methods are performed for periodic channel flow at a friction velocity based Reynolds number $Re_\tau = 200$. The normal and shear stress distributions and the turbulence intensities are compared with the DNS solution of Kim et al. [17].

* Corresponding author.
E-mail address: r.freitas@aia.rwth-aachen.de (R.K. Freitas).

0045-7930/$ - see front matter © 2011 Elsevier Ltd. All rights reserved.
doi:10.1016/j.compfluid.2011.02.019

Nomenclature

Symbol table

c_S	isothermal speed of sound
f_i	particle distribution function
F_i	modified equilibrium distribution
m	mass
Ma	mach number
$\vec{r}$	position vector
Re	Reynolds number
Re_τ	friction velocity based Reynolds number
t	time
t_P	weighting factors for the distribution function
u_i	velocity vector
y^+	nondimensional wall distance

Abbreviations

BGK	Bhatnagar–Gross–Krook
CLB	cascaded Lattice-Boltzmann method
DNS	direct numerical simulation
LBM	Lattice-Boltzmann method
MRT	multiple-relaxation-time
SGS	subgrid scale

Greek symbols

α,β	index for space dimension
δ	Lattice spacing or Kronecker symbol
ρ	density
ξ_i	molecular velocity, lattice velocity
ω	collision frequency

2. Numerical methods

2.1. BGK method

The well known BGK equation reads

$$f_i(\vec{r}+\xi\delta t, t+\delta t) = f_i(\vec{r},t) + \omega\delta t\cdot(F_i(\vec{r},t) - f_i(\vec{r},t)) \quad (1)$$

with the equilibrium distribution function $F_i(\vec{r},t)$

$$F_i(\vec{r},t) = \rho t_p\left[1+\frac{\xi_{i,\alpha}u_\alpha}{c_S^2}+\frac{u_\alpha u_\beta}{2c_S^2}\left(\frac{\xi_{i,\alpha}\xi_{i,\beta}}{c_S^2}-\delta_{\alpha,\beta}\right)\right], \quad (2)$$

where $\alpha = 1, 2, 3$ and $\beta = 1, 2, 3$ represent the space dimensions and $\delta_{\alpha\beta}$ is the Kronecker delta. The coefficients t_P are weighting factors to be chosen such that macroscopic symmetry and conservation of mass and momentum are satisfied. For the 19 velocity model one obtains $t_0 = 1/3$, $t_1 = 1/18$, $t_2 = 1/36$, and $c_S = \sqrt{c^2/3}$, and for the 27 velocity model $t_0 = 8/27$, $t_1 = 2/27$, $t_2 = 1/54$, $t_3 = 1/216$, and $c_S = \sqrt{c^2/3}$, where the index describes the square modulus of the discrete velocities ξ_i and $c = 1$. Details of the derivation of the weighting factors are given in [18]. The macroscopic flow values for mass and momentum are determined by summation over the distribution functions

$$\rho = \sum_{i=1}^{i=i_{max}} f_i = \sum_{i=1}^{i=i_{max}} F_i, \quad (3)$$

$$\rho u_\alpha = \sum_{i=1}^{i=i_{max}} \xi_{\alpha,i} f_i = \sum_{i=1}^{i=i_{max}} \xi_{\alpha,i} F_i, \quad (4)$$

2.1.1. Incompressible BGK model

The standard LBM describes weakly compressible flows, since the Taylor series expansion of the Maxwell equilibrium distribution is performed at Mach number zero. To further decouple the pressure and the density, i.e., to obtain a solution method for incompressible flows, a modified equilibrium distribution has been chosen as presented by Zou et al. [19]. The modified equilibrium distribution reads

$$F_i(\vec{r},t) = t_p\left[\rho+\frac{\xi_{i,\alpha}u_\alpha}{c_S^2}+\frac{u_\alpha u_\beta}{2c_S^2}\left(\frac{\xi_{i,\alpha}\xi_{i,\beta}}{c_S^2}-\delta_{\alpha,\beta}\right)\right]. \quad (5)$$

2.2. The MRT method

To extend the stability of the LBM a general collision operator has been proposed [2] and further improved and analyzed in [20,21]. While the propagation step is the same for the BGK and the MRT model, the collision operator of the MRT-algorithm executes the relaxation in moment space, thus linking the relaxation constants to the moments of the distribution functions which represent physical flow properties. By this a decoupling of conserved and non-conserved moments is achieved to enhance the stability and accuracy of the method. The moment representation of the LBM leads to a number of free parameters, including the relaxation rates. The interaction of the hydrodynamic second-order moments and other higher-order moments depends on this choice of free parameters. For the three-dimensional case D'Humieres et al. proposed a set of parameters based on linear analysis of the linearized hydrodynamic equations [21]. This proposed parameter set has also been applied for turbulence simulation via the MRT-LBM in [12]. In our study, we use the choice of free parameters for the MRT method as given in [12], without a subgrid scale model. Details for the linear analysis and its validity are given in [20,21].

2.3. The CLB method

The CLB method has been proposed by Geier et al. [3]. Similar to the MRT method the CLB method is based upon a moment representation of the collision operation. The construction of the higher-order moments is based on the lower moments. This means that the post-collision moments of lower order are used for the calculation of the higher-order moments. A collision cascade is established, which includes also the higher moments of the discrete velocity set up to fourth order, i.e., non-hydrodynamic moments. In [3] the authors argue that the instability of the Lattice-Boltzmann method at higher Reynolds numbers is a result of the inability to properly capture short wavelength oscillations. They state these short wavelength oscillations are correctly described by the inclusion of the higher-order moments. The CLB collision operator has a rather high complexity compared to the MRT or even the BGK operator, especially since the authors insist on a 27 velocity discretization for an accurate hydrodynamic behavior of the method.

2.4. Boundary conditions

2.4.1. Periodic boundaries

Since the development of fully turbulent flow takes quite a number of iteration steps it is common practice to use periodic boundary conditions, especially for well analyzed cases as periodic channel flow. Such periodic boundaries are imposed for the

channel flow on the inflow and outflow boundaries and in the spanwise direction.

2.4.2. No-slip conditions

No-slip conditions are simulated by halfway bounce-back formulations for the channel walls as described in Bouzidi et al. [22], which is the most commonly used boundary condition and gives second-order accuracy for MRT and BGK.

2.4.3. Sliding walls

The driven cavity at yaw test case, introduced by Povitsky [23], requires the formulation of sliding walls. The simulation of moving walls can be accurately treated by a bounce-back method proposed in [24]. This delivers good results for the BGK19 and BGK27 methods but fails for the MRT and CLB method, therefore we adopt the equilibrium distribution based formulation of D'Humieres et al. in [21], which allows stable computations for all methods, despite the fact that it introduces an unphysical pressure and momentum transfer. The formulation for the sliding wall boundary reads

$$f_\alpha = t_p \rho_0 \frac{\xi_\alpha u_{wall}}{c_s^2}. \tag{6}$$

2.4.4. External forcing

For the turbulence simulations, an external forcing term f_{force}, i.e., a source term in the LBM as described in [25] and applied in [26], is used

$$f_{force} = \frac{F_\alpha}{m} \rho \frac{1}{c_S^2} \xi_i, \tag{7}$$

where m, ρ, c_S are the mass, density, and the speed of sound and ξ_i represents the discrete velocity corresponding to the distribution function direction i. Instead of using an external force the pressure or density drop can also be simulated directly. This has been done in [27] and was found to deliver equally accurate results. In this study we used the external forcing approach.

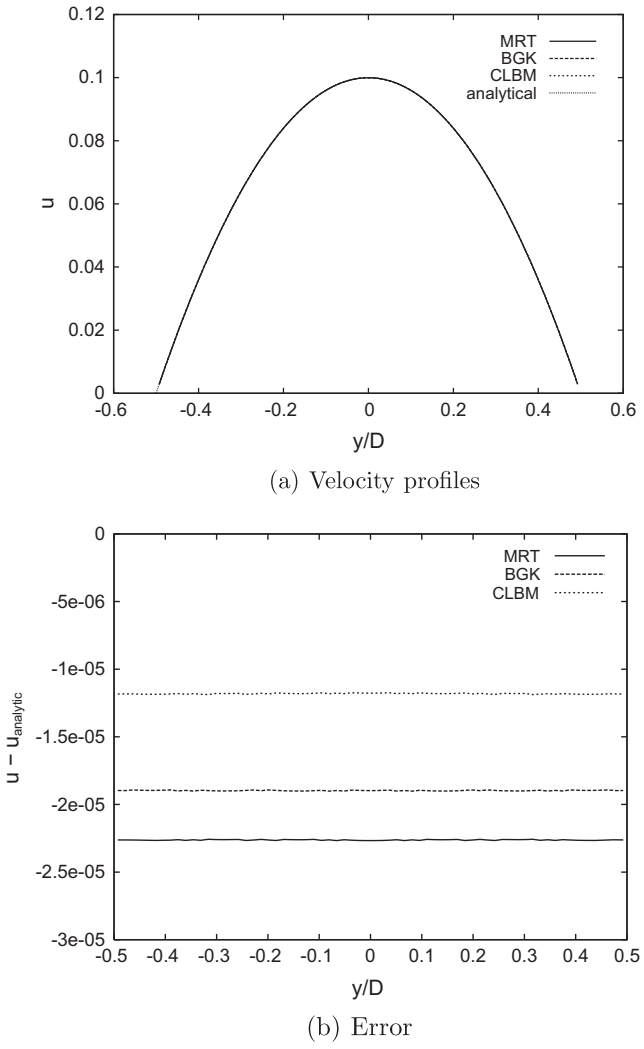

Fig. 1. Laminar velocity profiles and error for plane Poiseuille flow.

3. Validation

In this section we validate our implementation to ensure that it delivers correct results and that the findings in the following section are not due to flaws in the implementation but really are results of each corresponding method.

3.1. Plane poiseuille flow

To validate the different implementations, plane Poiseuille flow at a Reynolds number of 200 is calculated. The distance between the two infinite plates is resolved with 68 cells. In Fig. 1a the velocity profiles for the different methods are compared after $t = 1e5\Delta t$. The different profiles collapse. However, when the error is analyzed by subtracting the analytic solution minor differences show up as can be seen in Fig. 1b. Although the absolute error of the CLB method is slightly smaller than that of the MRT and BGK method it still has an equal order of magnitude and it can be stated that all models perform equally well for the plane Poiseuille flow test case with the chosen setup. Furthermore, for this simple test case the 19 and 27 velocity BGK models deliver the same results up to machine accuracy. Therefore, the velocity distributions in Fig. 1 do not evidence any difference. The results in Fig. 1 show that the correct flow physics is captured by all methods. Clearly, the accuracy for this steady case is further improved when the number of timesteps is increased and when advanced boundary conditions are applied. However, since we are interested in the investigation of a highly unsteady flow, an exact solution for the Poiseuille flow is not pursued at this point.

3.2. Three-dimensional lid driven cavity at yaw

In [21] the authors used the three-dimensional lid driven cavity flow at yaw discussed in detail in [23] to study the performance of the MRT model with 15 discrete velocities. The same test case is used in this study for the validation of the different methods to check the correctness of the implementation of the various models. The solutions for the BGK19, BGK27, MRT, and CLB method are compared with the results by Povitsky [23] obtained by the commercial Finite Volume solver FLUENT. The test case setup is similar to that in [21], i.e., the diagonally driven cavity is discretized with on a uniform 52^3 mesh and the velocity vector patterns at different cavity height based Reynolds numbers 700 and 2000 are compared with the results in [23]. Our results confirm the earlier findings of D'Humieres et al. [21], i.e., the BGK and MRT methods with second-order accuracy show very good agreement with the reference case at $Re = 700$ as evidenced by the velocity vector patterns in Fig. 2. The results for the BGK19 and BGK27 at $Re = 700$ method match. The position of the centers of the vortices differ less than 3% of the reference length which is defined by the length of the cavity height. As has been stated in [21] the MRT method reveals a much higher stability than the BGK method. While the latter does not

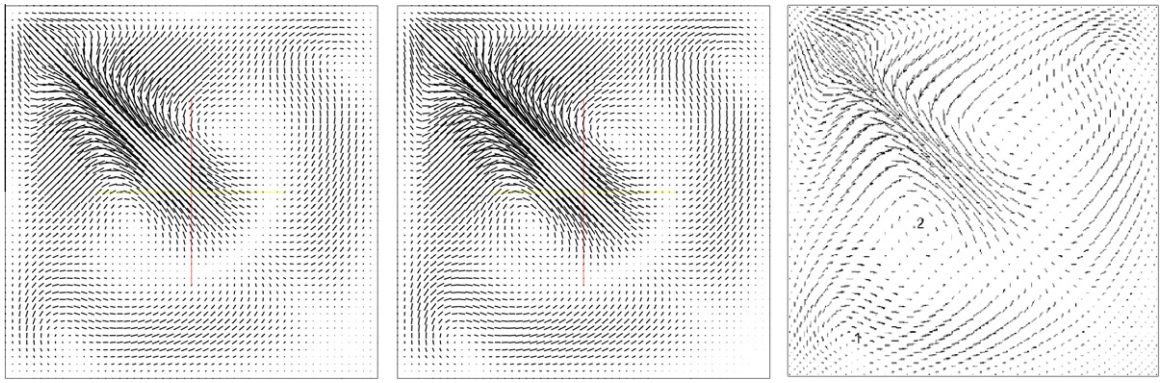

Fig. 2. Velocity patterns for cavity flow at yaw at $Re = 700$ from left to right: BGK19 model, MRT model, reference case taken from Povitsky [23].

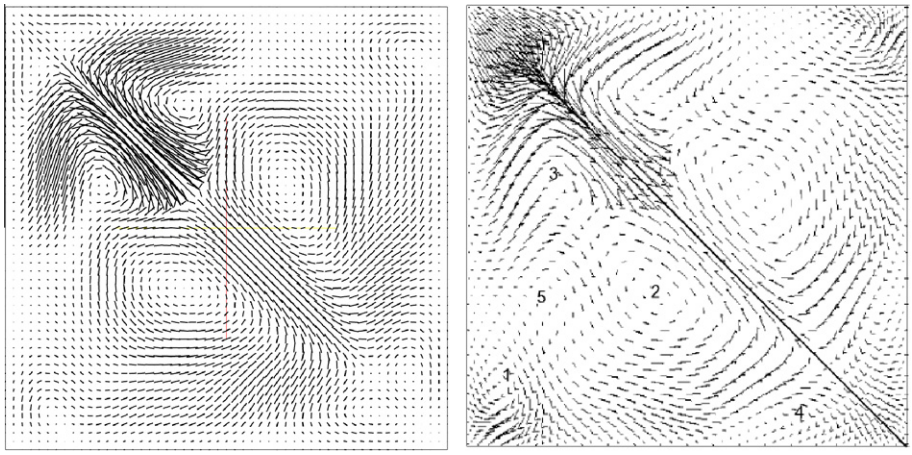

Fig. 3. Velocity patterns for cavity flow at yaw at $Re = 2000$. MRT model (left), reference case [23] (right).

give a stable result beyond $Re = 1000$, the MRT method still does well at $Re = 2000$ as can be seen in Fig. 3. The distance between the centers of the vortices of the present MRT model differs from the reference case by approximately 10% based on the reference length. Although the CLB method with 27 velocities is stable for at least a Reynolds number of $Re = 700$, the result shown in Fig. 4 resembles that of the $Re = 2000$ finding of Povitsky and not that of the $Re = 700$ solution. The comparison of this result with the findings in Fig. 2 indicates that the CLB method possesses a lower inherent numerical diffusion than the BGK19 and the MRT models.

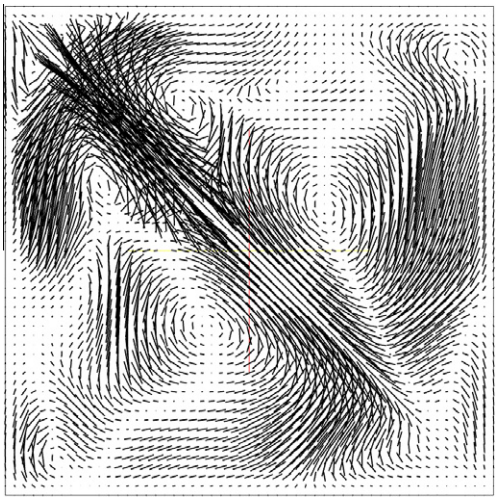

Fig. 4. Velocity patterns for cavity flow at yaw at Re 700 with CLB model.

4. Turbulent channel flow

The turbulent channel flow is simulated without a subgrid scale (SGS) model. The chosen resolution of $y^+ \approx 3 (y^+ \approx 1.5$ directly at the wall) is too coarse for a resolution of the smallest scales, to be more precise the resolution is in the range of approx. twice

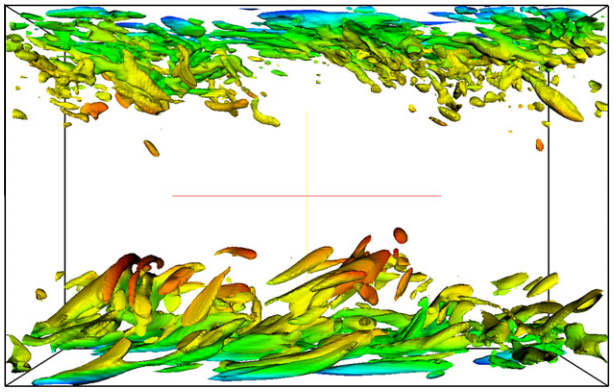

Fig. 5. λ_2-contours of the BGK19 simulation at $Re_\tau = 200$ (bottom) and $Re_\tau = 360$ (top).

the Kolmogorov length. Therefore, the computation can be considered an under resolved direct numerical simulation (DNS). However, the aim of this study is not to perform a highly resolved reference DNS, but to compare the performance of the different methods in terms of stability and accuracy using the same resolution for any method. It will be seen in the following results that the chosen test case already reveals some insight on the stability properties of the different methods.

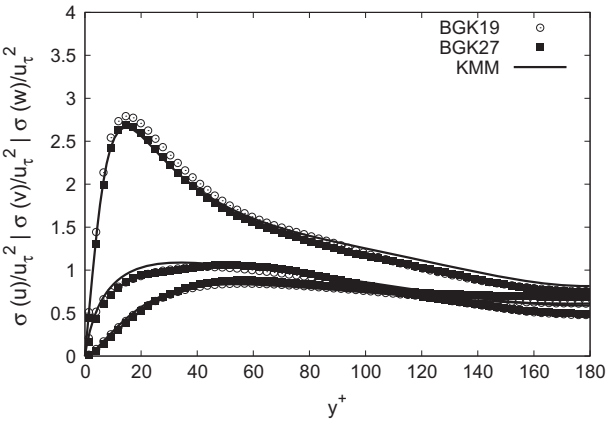

(a) Reynolds stress tensor

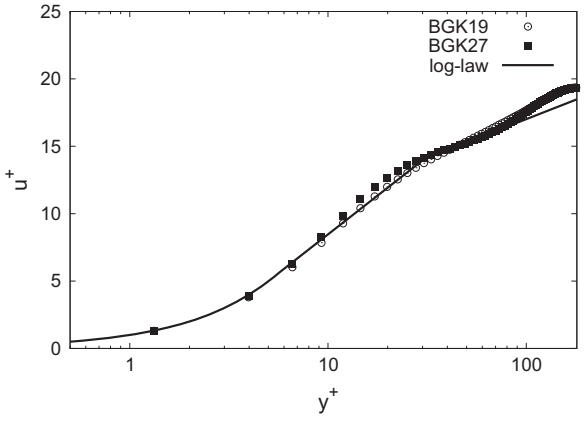

(b) Velocity profiles

Fig. 6. Normal components of the Reynolds stress tensor and mean velocity profile for BGK19 and BGK27 at $Re_\tau = 200$.

4.1. Initialization

For the BGK method, the simulations are initialized using a logarithmic profile and artificial velocity fluctuations. The fluctuations are computed to deliver a divergence-free velocity field. Running the simulation for several time units leads to a fully turbulent flow. For the periodic channel test case a time unit is defined as the time a fluid particle at mean axial velocity takes to travel the half width H of the channel. This straightforward initialization method works for the BGK method but does not lead to satisfactory results for the CLB and MRT method. For the MRT method an initialization method has been proposed in [28]. This special initialization method creates a consistent velocity and pressure field and also gives non-equilibrium distributions which is necessary if the hydrodynamic moments of the initial flow field have non-vanishing gradients. However,in this study the CLB and MRT simulations are initialized using a fully turbulent solution of the corresponding BGK methods, which delivers the correct non-equilibrium values and correct physics, i.e. consistent macroscopic flow field. The fully turbulent state of the BGK solution is again evidenced by comparing the statistics with DNS data from Kim et al. [17].

4.2. Periodic channel flow

A Reynolds number based on the friction velocity and the channel half-height (H) $Re_\tau = 180$ is applied in [17]. In this study, a slightly higher Reynolds number $Re_\tau = 200$ is considered and therefore a linear rescaling of the Reynolds stress components is used in Fig. 6. Two Mach numbers, $Ma = 0.05$ and $Ma = 0.1$, have been prescribed. Since the findings do coincide only $Ma = 0.05$ solutions are presented. The computational domain of the channel flow possesses a length ($L = \pi H$), height ($2H$), and width ($W = 0.289\pi H$), according to the minimum specifications for a periodic channel given by Jiménez and Moin [29]. To resolve the flow field a mesh consisting of $211 \times 135 \times 61$ equidistant cells in streamwise, normal and spanwise direction is used.

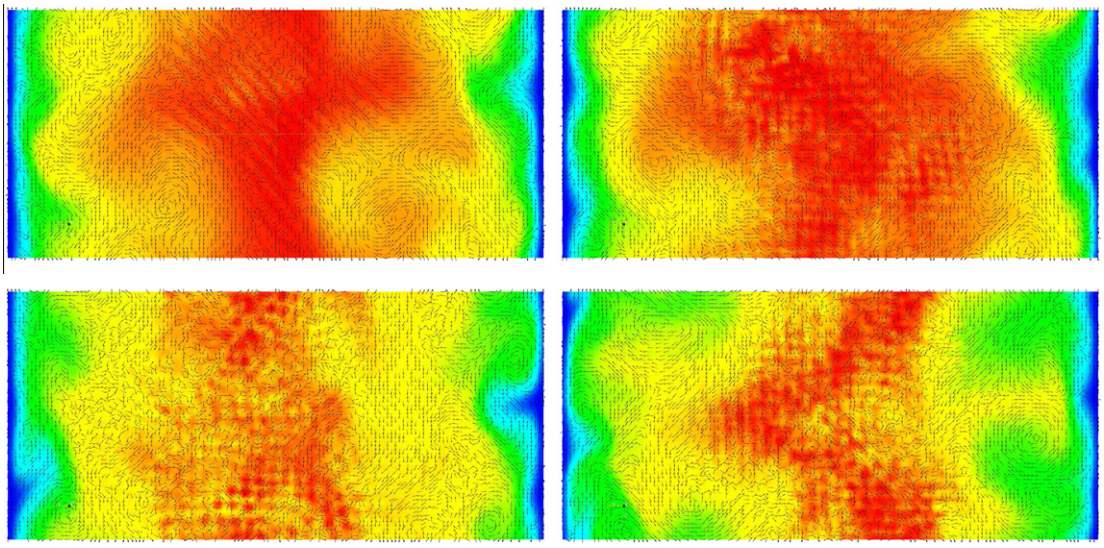

Fig. 7. From the left to right and top to bottom. Velocity vectors and contours after 8, 11, 22 and 44 time units for MRT channel simulation.

4.2.1. BGK method

The turbulent character of the flow simulation is evidenced by the λ_2 [30] contours in Fig. 5, which give an impression of the vortical structures at $Re_\tau = 200$ and $Re_\tau = 360$.

A more quantitative result is obtained by the components of the Reynolds stress tensor and the mean velocity profiles in Fig. 6. The distributions of the BGK19 and BGK27 method show a good agreement with the reference DNS data and the analytical solution, respectively. However, it is evident that especially the peak value of the streamwise component of the Reynolds stress tensor is more accurately determined by the BGK27 approach.

4.2.2. MRT method

Following the results from our validation and according to the superior results achieved by the MRT method and the CLB method, a similar quality should be expected for the periodic channel flow. However, surprisingly this is not the case. While the BGK19 and BGK27 methods reach a fully turbulent state and give reasonable statistics for the rather coarse grid, the MRT method revealed an unphysical behavior in the simulation of the periodic channel test case at the given Reynolds number. After some time units an initially fully turbulent flow field taken from a BGK19 simulation becomes unphysical, i.e., spurious oscillations occur which contaminate the simulation. In Fig. 7 the decay of the solution as a function of time is evident. Note, to ensure that the observed oscillations are not due to a flawed implementation of the MRT-algorithm we applied the parameter set given in [21] which reduces the MRT model to the BGK model. With this reduced model no oscillations were observed, i.e. the results were of the same quality as that of the original BGK implementation. Furthermore, to remedy the problems we increased the grid resolution to $421 \times 269 \times 123$ equidistant cells in streamwise, normal and spanwise direction and performed the MRT simulation again, yet again the oscillations did show up.

4.2.3. CLB method

The CLB channel simulation becomes laminar after several time units. At a higher Reynolds number of $Re_\tau = 360$ the simulation remains turbulent but strong unphysical fluctuations occur at the walls as evidenced by the instantaneous velocity field in Fig. 8. Although it could be argued that the simulation is stable and might give good qualitative results, the negative impact of these fluctuations on the validity of the flow simulation shows up when the time averaged solution is considered. Looking at the corresponding Reynolds stress tensor in Fig. 9, the unphysical flow behavior in the near wall region for $y^+ < 25$ becomes obvious. Running the CLB simulation at the higher Reynolds number of $Re_\tau = 360$ for 50 time units and then gradually reducing the Reynolds number to $Re_\tau = 180$ finally results in a stable simulation. Further investigations will analyze the susceptibility of CLB to the initial conditions and moreover, the generation of the fluctuations the pattern of which is evidenced in Fig. 8 is to be clarified.

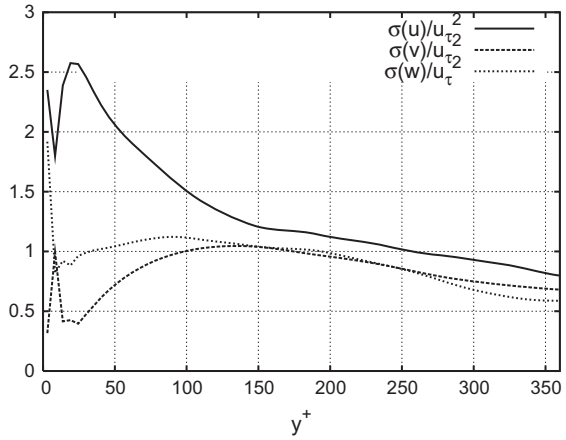

Fig. 9. Components of the Reynolds stress tensor for the CLB channel simulation.

5. Conclusion

The possibility to simulate wall-bounded turbulent flows at moderate Reynolds numbers has been investigated, using three

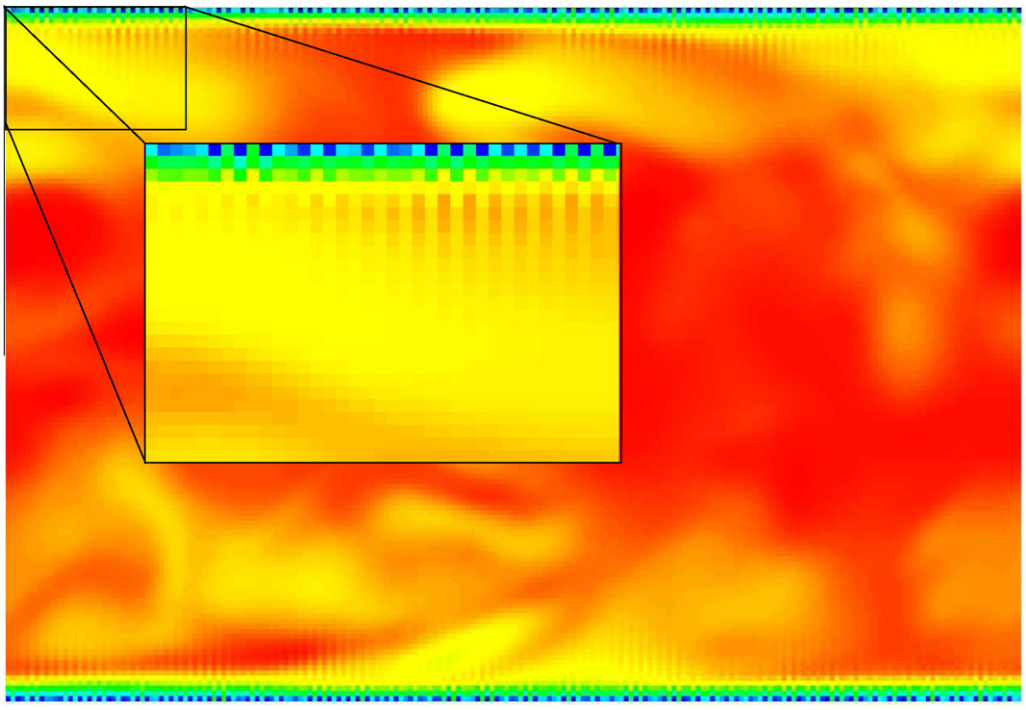

Fig. 8. Contours of the instantaneous velocity field for the CLB channel simulation.

Lattice-Boltzmann Methods, namely the BGK, the MRT, and the CLB method. The BGK method has been simulated with 19 and 27 discrete velocities, the CLB method with 27 discrete velocities and the MRT with 19 discrete velocities. The three-dimensional lid driven cavity at yaw has been used as a reference case to confirm the correct three-dimensional behavior of the methods. This test case revealed strong discrepancies in the boundary condition treatment of the different methods. Therefore, it was considered inadequate to accurately compare the various methods.

Stable and physically meaningful turbulent channel flow simulations have been performed for the BGK method. The BGK19 and BGK27 methods have shown similar results in the analysis of the Reynolds stresses. They have been in good agreement with the DNS data of Kim et al. [17]. Note, however, that regarding the peak value of the streamwise normal Reynolds stress the BGK27 has possessed a smaller deviation from the DNS data than the BGK19 method. The MRT method with the parameter set from [31] displays spurious artifacts for the periodic channel flow especially off the walls. The CLB model remained stable for the turbulent channel flow but it generated too much artificial viscosity, resulting in a relaminarized flow for the turbulent channel flow at $Re_\tau = 200$. Further computations showed that a stable turbulent flow could be achieved if the initialization has been based on a higher Reynolds number. The method also had problems with the simple bounce-back wall boundary condition at higher Reynolds numbers. Note, no subgrid scale model has been used in any of the performed simulations.

For the presented test case and the applied simulation setup only the BGK methods showed a good agreement with the aforementioned DNS data. We would like to stress that due to the strong dependence of the stability of the methods on the investigated problems it is hard to give a general prediction on the overall performance of the methods.

Acknowledgments

We would like to thank Martin Geier for providing his implementation of the three-dimensional CLB collision operator and his helpful comments and interest in our work. This work was funded by the German Research Foundation (DFG) under grant *SCHR 309/22*.

References

[1] Bhatnagar PL, Gross EP, Krook M. A model for collision processes in gases. I. Small amplitude processes in charged and neutral one-component systems. Phys Rev 1954;94(3):511–25.
[2] D'Humieres D. Generalized lattice-Boltzmann equation. In: Rarefied gas dynamics: theory and simulations. Progress in astronautics and aeronautics 1992;159:450–458.
[3] Geier M, Greiner A, Korvink JG. Cascaded digital lattice Boltzmann automata for high Reynolds number flow. Phys Rev E 2006;73(6):066705.
[4] Geier M, Greiner A, Korvink JG. Properties of the cascaded lattice Boltzmann automaton. Int J Mod Phys C 2007;18(4):455–62.
[5] Geier M. De-aliasing and stabilization formalism of the cascaded lattice Boltzmann automaton for under-resolved high Reynolds number flow. Int J Numer Methods Fluids 2007;56(8):1249–54.
[6] Asinari P. Generalized local equilibrium in the cascaded lattice Boltzmann method. Phys Rev E 2008;78:016701.
[7] Karlin IV, Ferrante A, Öttinger HC. Perfect entropy functions of the lattice Boltzmann method. Europhys Lett 1999;47(2):182–8.
[8] Keating B, Vahala G, Yepez J, Soe M, Vahala L. Entropic lattice Boltzmann representaions required to recover Navier-Stokes flows. Phys Rev E 2007;75:036712.
[9] Brownlee RA, Gorban AN, Levesley J. Nonequilibrium entropy limiters in lattice Boltzmann methods. Physica A 2007;387:385–406.
[10] Spasov M, Rempfer D, Mokhasi P. Simulation of a turbulent channel flow with an entropic Lattice Boltzmann method. Int J Numer Methods Fluids 2009;60:1241–58.
[11] Chikatamarla SS, Frouzakis CE, Karlin IV, Tomboulides AG, Boulouchos KB. Lattice Boltzmann method for direct numerical simulation of turbulent flows. J Fluid Mech 2010;656:298–308.
[12] Yu H, Luo LS, Girimaji SS. LES of turbulent square jet flow using an MRT lattice Boltzmann model. Comput Fluids 2006;35(8/9):957–65.
[13] Higuera FJ, Succi S, Benzi R. Lattice gas dynamics with enhanced collisions. Europhys Lett 1989;9:663–8.
[14] Amati G, Succi S, Piva R. Massively parallel lattice-Boltzmann simulation of turbulent channel flow. Int J Mod Phys 1997;8(4):869–77.
[15] Toschi F, Amati G, Succi S, Benzi R, Piva R. Intermittency and structure functions in channel flow turbulence. Phys Rev Lett 1999;82(25):5044–7.
[16] Benzi R, Succi S, Vergassola M. The lattice Boltzmann equation: theory and applications. Phys Rep 1992;222(3):145–97.
[17] Kim J, Moin P, Moser R. Turbulence statistics in fully developed channel flow at low Reynolds number. J Fluid Mech 1987;177:133–66.
[18] Succi S. The lattice Boltzmann equation for fluid dynamics and beyond. Numerical mathematics and scientific computation. Oxford: Clarendon Press; 2001.
[19] Zou Q, Hou S, Chen S, Doolen GD. An improved incompressible Lattice Boltzmann model for time-independent flows. J Stat Phys 1996;81:35.
[20] Lallemand P, Luo LS. Theory of the lattice Boltzmann method: dispersion, dissipation, isotropy, Galilean invariance, and stability. Phys Rev E 2000;61:6546–62.
[21] D'Humières D, Ginzburg I, Krafczyk M, Lallemand P, Luo L-S. Multiple-relaxation-time lattice Boltzmann models in three dimensions. Roy Soc Lond Philos Trans Ser A 2002;360(March):437–51.
[22] Bouzidi M, Firdaouss M, Lallemand P. Momentum transfer of a Boltzmann-lattice fluid with boundaries. Phys Fluids 2001;13(11):3452–9.
[23] Povitsky A. Three-dimensional flow in cavity at yaw. Nonlinear Anal 2005;63(5–7):e1573–84. November.
[24] Bouzidi M, Firdaouss M, Lallemand P. Momentum transfer of a Boltzmann-lattice fluid with boundaries. Phys Fluids 2001;13:452–9.
[25] Hänel D. Molekulare Gasdynamik. Springer; 2004.
[26] Freitas RK, Meinke M, Schröder W. Turbulence simulation via the lattice-Boltzmann method on hierarchically refined meshes. In: Proceedings ECCOMAS CFD 2006; 2006.
[27] Freitas RK, Meinke M, Schröder W. Investigation of lattice Boltzmann methods for LES. Progress in turbulence, vol. II. Springer; 2005.
[28] Mei R, Luo L, Lallemand MP, d'Humieres D. Consistent initial conditions for lattice Boltzmann simulations. Comput Fluids 2006;35:855–62.
[29] Jiménez J, Moin P. The minimal flow unit in near wall turbulence. J Fluid Mech 1991;225:213–40.
[30] Jeong J, Hussain F. On the identification of a vortex. J Fluid Mech 1995;285:69–94.
[31] Yu H, Girimaji SS, Luo LS. DNS and LES of decaying isotropic turbulence with and without frame rotation using lattice Boltzmann method. J Comput Phys 2005;209:599–616.